Probing the intergalactic magnetic field through observations of high-energy gamma rays produced by electromagnetic cascades

B Bisschof, B van Soelen and P J Meintjes

Department of Physics, University of the Free State, Bloemfontein, South Africa

E-mail: bisschoffb@ufs.ac.za

Abstract. Currently there is limited knowledge related to the origin of the intergalactic magnetic fields (IGMF) that permeate the space between galaxies, galaxy clusters and cosmic voids. Understanding the origin of the IGMF is a crucial component in models of galaxies and galaxy cluster formation. This magnetic field can be probed indirectly by its effect on electromagnetic cascades initiated by gamma-gamma absorption of very-high-energy (VHE) gamma rays, produced in blazars, due to its interaction with the extragalactic background light (EBL). The electron-positron pairs produced via this process interact with the intergalactic magnetic field (IGMF) and can be deviated from their original path. These pairs can then Compton-scatter off the cosmic microwave background (CMB) to produce high-energy (HE) gamma rays that may be detected by, e.g., *Fermi*-LAT. The strength of this signal strongly depends on the IGMF strength (B) and the coherence length (λ_B). This secondary gamma-ray emission would be superimposed on the blazars' intrinsic gamma-ray spectrum. A selection of bright blazars will be re-analysed using the upgraded Pass 8 analysis pipeline, to search for this secondary component. This will be used to place constraints on the IGMF strength. The initial results from this project, namely the *Fermi*-LAT analysis of a selection of candidate blazars for this study are presented. The results showed that the light curves and the spectral shape of the SEDs showed negligible variability and that the spectral parameters and fluxes values overlaped within one standard deviation within the results from Finke et al. (2015). This indicates that these are appropriate sources to use for further modelling.

1. Introduction

For a variety of astrophysical objects, like galaxies and galaxy clusters, magnetic fields play a very important role. Observations of Faraday rotation and Zeeman splitting of atomic lines in the radio band and the observations of the polarization of starlight in the optical band, established the existence of galactic magnetic fields with strengths of $1-10$ μG [1, 2]. The cores of galaxy clusters also have magnetic fields of similar strengths [3]. Recently magnetic fields of $10^{-8}-10^{-7}$G have also been discovered outside galaxies and galaxy clusters in the intergalactic space [4, 5].

The galactic magnetic fields, in galaxies and galaxy clusters, are assumed to be caused by the amplification of the weak seed fields that are of cosmological origin. The mechanism of the amplification, nature and origin of these weak seed fields are currently still unknown. By making measurements of these initial seed fields, this process can be constrained. This intergalactic magnetic field (IGMF) can be indirectly measured with gamma-ray telescopes based on its

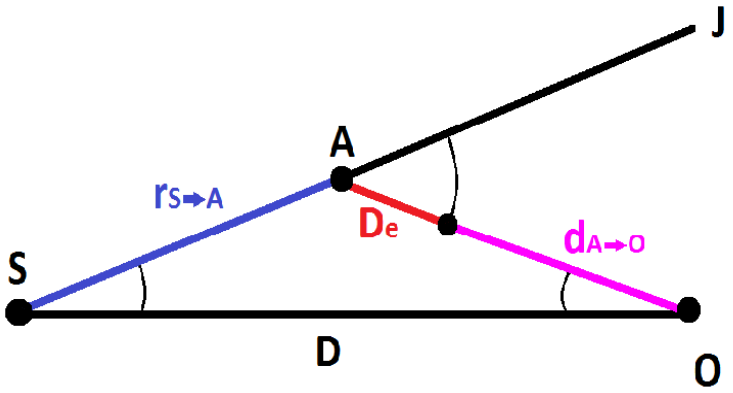

Figure 1. The electromagnetic cascade process occurs close to the blazar jet situated at point S and separated by the distance D from the observer on Earth at the point O. The line $r_{S\to A}$ represents the distance the VHE photons, originating from the blazar, travel before interacting with the EBL at point A to form electron-positron pairs. D_e is the electron cooling distance which the electron/positron travel, while being deviated from the original path by an angle δ, before interacting with a CMB photon and upscattering these photons to high-energies. The HE photons then travel a distance $d_{A\to O}$ before finally reaching the observer at point O.

effect on the emission originating from electromagnetic cascades from extragalactic sources such as Blazars [6, 7, 8, 9, 10].

The range of the IGMF parameters, such as the strength (B) and the coherence length (λ_B), can be found, based on the knowledge of the sensitivity of existing and future gamma-ray telescopes, with two available measurement techniques (Timing [6, 8] or imaging [7, 9, 10] of the gamma-ray cascade signal). The timing method measures the effect of the IGMF on the arrival times of gamma rays from extragalactic sources. The imaging method measures the effect of the IGMF on the angular profile of the extended emission coming from blazars. In the imaging method the sources need to be non-variable in flux because the modelling requires a stable emission output from the blazar source. The timing analysis becomes uncertain for determining magnetic field strengths larger than 10^{-18} G when the delay times of the secondary spectrum becomes large, up to a 100 years for magnetic field strengths $>10^{-16}$ G [11]. Thus its much more practical to measure the angular extend of a source than to measure the time delays in flaring events.

For this analysis, stable sources are required, so the SEDs are not complicated by flaring or variability events. As the first step in this project we have investigated the stability of three potential sources for this analysis. In section 2 we discuss the pencil beam model (model for non-variable sources) for the electromagnetic cascade process that occurs in the blazar jets and how these cascade signals are influenced by the IGMF. Then in section 3 to we explain how FermiPy was used to reduce and analyze the data from three different blazar sources. In section 4 the spectral index and flux variability of these three sources were determined and then compared to the results of Finke et al. (2015) [12]. Finally we discuss our obtained results and the following steps that will be taken to model and put constraints on the IGMF parameters (B) and (λ_B).

2. Theory

Consider a blazar positioned at a point S as shown in figure 1. The AGN emits a narrow beam of very-high-energy (VHE) gamma rays along SJ that is misaligned with the line of sight SO. The VHE photons are absorbed, after traveling a distance $r_{S\to A}$, at point A through gamma-

Table 1. SED model fitting results obtained from Finke et al. (2015) for the three different blazar sources: 1ES 1218+304, 1ES 0414+009 and 1ES 1101-232.

Source Name	Redshift	TS	Flux[10^{-9}.cm^{-2}.s^{-1}]	Spectral Index	Variability Index
1ES 1218+304	0.182	1690	15.6±1.5	1.68±0.03	92
1ES 0414+009	0.287	127	3.10±0.99	1.74±0.10	56
1ES 1101-232	0.186	75.6	1.57±0.67	1.63±0.14	37

gamma absorption, due to interaction with lower-energy extragalactic background light (EBL) photons, and electron-positron pairs are created [6, 7]. These pairs then traverse a distance D_e , in the direction of O, in the presence of the intergalactic magnetic field (IGMF) before colliding with a lower energy cosmic microwave background (CMB) photon. The two charged particles can deviated from their original path by an angle δ while traversing space in the presence of the IGMF. The deflection angle δ strongly depends on the strength and spacial structure of the magnetic field. If the magnetic field lines are tangled up in a region smaller than the electron cooling distance D_e, then the charged particles will follow a random walk process rather than a circular deviation path in the presence of the IGMF. This spacial structure of the IGMF is described by the coherence length of the IGMF which is defined as the average distance in which the magnetic field changes its orientation by 90 degrees. After this CMB photons are up-scattered to high-energy photons by the electron-positron pairs. This will result in an attenuation and energy shift of the original gamma-ray emission profile.

The power of the Inverse Compton (IC) emission from the electron-positron pairs is given by [13],

$$\frac{dP_{IC}}{dr} = \frac{E_{\gamma 0} N_0}{D_{\gamma 0}} e^{-\frac{r}{D_{\gamma 0}}}, \tag{1}$$

where N_0, $E_{\gamma 0}$ and $D_{\gamma 0}$ are the number of photons, energy and the mean free path of the primary gamma rays emitted from the blazar jet and r is the distance from point S to point A. The angle of deflection, caused by the interaction of the positron-electron pairs with the IGMF, for the secondary photon cascade for two different regimes is [14],

$$\delta(x) = \begin{cases} \frac{D_e}{R_L} \cong 3 \times 10^{-6}(1+z_{\gamma\gamma})^{-4}(\frac{B'}{10^{-18}\mathrm{G}})(\frac{E'_e}{10\mathrm{TeV}})^{-2}, D_e \ll \lambda'_B \\ \\ \frac{\sqrt{\lambda_B D_e}}{R_L} \cong 5 \times 10^{-7}(1+z_{\gamma\gamma})^{-2}(\frac{B'}{10^{-18}\mathrm{G}})(\frac{E'_e}{10\mathrm{TeV}})^{-\frac{3}{2}}(\frac{\lambda'_B}{1\mathrm{kpc}})^{\frac{1}{2}}, D_e \gg \lambda'_B, \end{cases} \tag{2}$$

where D_e is the electron cooling distance, R_L is the Larmor radius, $z_{\gamma\gamma}$ is the redshift at point A, B' and λ'_B are the IGMF strength and coherence length and E'_e is the redshift dependent electron energy.

Table 2. Spectral parameter results obtained with FermiPy for the blazar sources: 1ES 1218+304, 1ES 0414+009 and 1ES 1101-232.

Source Name	Redshift	TS	Flux[10^{-9}.cm^{-2}.s^{-1}]	Spectral Index
1ES 1218+304	0.182	3464.24	16.72±0.87	1.71±0.02
1ES 0414+009	0.287	257.11	5.04±0.94	1.91±0.07
1ES 1101-232	0.186	202.58	2.33±0.54	1.72±0.08

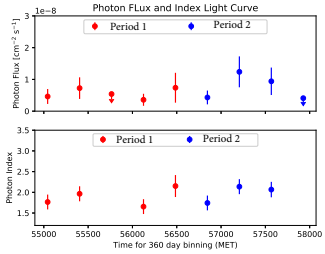

(a) Light curve for the source 1ES 0414+009 for the Period 1 (2008/08/04 to 2013/07/12) and Period 2 (2014/07/08 to 2018/01/01) time periods.

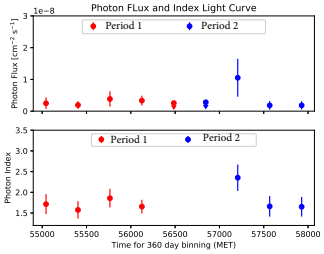

(b) Light curve for the source 1ES 1101-232 for the Period 1 (2008/08/04 to 2013/04/13) and Period 2 (2013/07/12 to 2018/01/01) time periods.

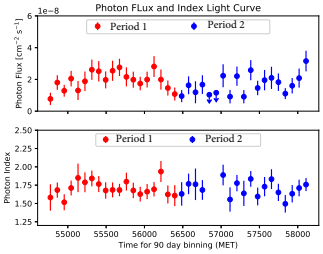

(c) Light curve for the source 1ES 1218+304 for the Period 1 (2008/08/04 to 2013/04/13) and Period 2 (2013/07/12 to 2018/01/01) time periods.

Figure 2. Lights curves for the sources a) 1ES 0414+009, b) 1ES 1101-232 and c) 1ES 1218+304. The data for two different time periods (Period 1, Period 2) are represented by red and blue data points in the figures above.

The IGMF strength and coherence length evolve with time as follows:

$$B'(z) \sim B_0(1 + z_{\gamma\gamma}^2)$$

$$\lambda'_B = \lambda_{B0}(1 + z_{\gamma\gamma})^{-1}$$

3. Data Reduction and Analysis

An investigation of this effect, of the IGMF supressing some of the high-energy inverse compton spectrum coming from blazar sources, was previously undertaken by Finke et al. (2015), however, their analysis was undertaken using Pass 7. As a first step in this project we have re-analysed three of the same sources using the newer Pass 8 analysis method (Table 1).

The high-energy photon data and spacecraft files for the sources 1ES 1218+304, 1ES 0414+009 and 1ES 1101-232 were extracted from the *Fermi* website. The high-energy data $(0.1 - 300\text{GeV})$ were extracted from 2008-08-04 00:00:00 to 2018-01-01 00:00:00 within a region of interest (ROI) radius of 30 degrees.

FermiPy (with *Fermi* Science Tools package verion: v11r5p3, and Python package version: 2.7.8) was then used to reduce and analyze the gamma-ray photon data. Fermipy was also used to perform the likelihood analysis on the three sources for different spectrum models. The normalization parameters of all the sources within a radius of 10 degrees from the center of the ROI were allowed to be free.

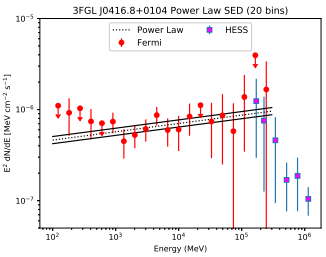

(a) SED for 1ES 0414+009 with Fermi and HESS data [15]. Red dots and pink squares represent the Fermi and HESS data respectively.

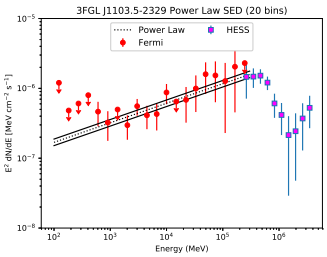

(b) SED for 1ES 1101-232 with Fermi and HESS data [16]. The data points are similarly presented as in a).

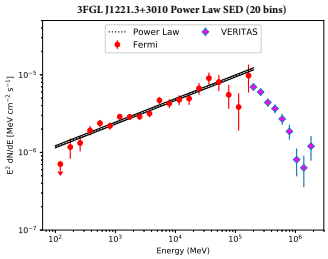

(c) SED for 1ES 1218+304 with Fermi and Veritas data [17]. Red dots and pink diamonds represent the Fermi and Veritas data respectively.

Figure 3. SEDs for the sources a) 1ES 0414+009, b) 1ES 1101-232 and c) 1ES 1218+304. The black dotted line represents the power-law model fit and the black filled lines represent the power-law model fit with one standard deviation from the dotted line fit.

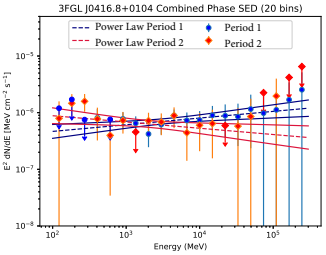

(a) Combined SED for 1ES 0414+009 with Fermi and HESS data for the Period 1 (2008/08/04 to2013/07/12) and Period 2 (2014/07/08 to 2018/01/01) time periods.

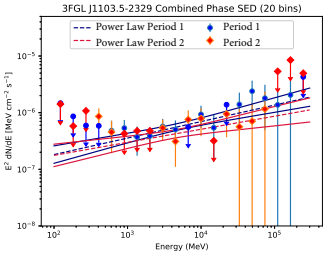

(b) Combined SED for 1ES 1101-232 with Fermi and HESS data for the Period 1 (2008/08/04 to 2013/04/13) and Period 2 (2013/07/12 to 2018/01/01) time periods.

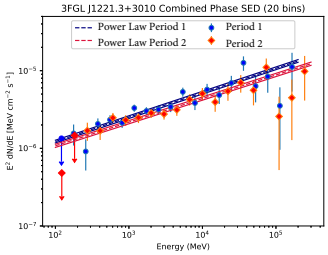

(c) Combined SED for 1ES 1218+304 with Fermi and Veritas data for the Period 1 (2008/08/04 to 2013/04/13) and Period 2 (2013/07/12 to 2018/01/01) time periods.

Figure 4. Combined SEDs for different time periods (Period 1 and Period 2) represented in the figures (blue dots and red diamonds) for the sources a) 1ES 0414+009, b) 1ES 1101-232 and c) 1ES 1218+304. Both time period peroids (Period 1 and Period 2) are fitted with a power-law model, with one standard deviation, reperesented by the dotted and filled lines respectivily (navy and maroon).

4. Results

The variability of each source has been investigated by producing light curves shown in figure 2. SEDs were also constructed during periods of higher and lower activity to compare whether the SEDs remained sufficiently stable and are shown in figure 3 for each source. A power-law, power-law with a super exponential cut off, log parabola, broken power-law and the smooth broken power-law spectrum models were tested for goodness-of-fit. The power-law spectrum model had the overall best Log Likelihood and test statistics (TS) values and also a better fit to the high-energy data points. For each blazar source a light curve, spectral index plot, SED plot and a combined SED plot for different time periods (Period 1 and Period 2) of the light curves, were produced (figure 4). These two time periods were chosen such that Period 1 and Period 2 had a maximum difference in there average spectral index values. All the SED and light curve plots showed little variability in the spectral index value, and the slopes of the spectrum

Power law models in the SED plots, and flux values. Thus all the investigated sources can be considered sufficiently non-variable for the future modelling. The spectral values obtained from all the sources are also consistent with those obtained by Finke et al. (2015).

5. Conclusion

The results from all the sources above, for the test statistic (TS) value integrated flux and the spectral index, are all within one standard deviation in agreement with the results obtained from the Finke et al. (2015) paper. The errors we have obtained are smaller because of the much higher TS values. This is because we have used approximately 9.5 years of data with Pass 8 where as Finke et al. (2015) used approximately 6 years of data with Pass 7. The spectral shape of the sources during different variable time periods (Period 1 and Period 2) in figure 2, showed little variability and the difference in spectral index between the two time periods lies within one standard deviation of one another and the spectral index for the full SED in figure 3. Thus our three sources are stable enough to model the IGMF affecting the VHE cascade spectra of these sources and place constraints on the IGMF strength and coherence length. Data analysis for an additional sample of sources is currently in progress. After this is completed a model based on the work of Arlen et al. (2014) will be developed with the use of the Monte Carlo code from Kachelrieß et al. (2012) to compare to the Fermi data. We will use this to place constraints on the IGMF.

References

[1] Kulsrud R M and Zweibel E G 2008 *Rept. Prog. Phys.* **71** 0046091
[2] Beck R 2009 *AIP Conf. Proc.* **1085** 83
[3] Carilli C L and Taylor G B 2002 *Ann. Rev. Astron. Astrophys.* **40** 319
[4] Xu Y, Kronberg P P, Habib S and Dufton Q W 2006 *Astrophys. J.* **637** 19
[5] Kronberg P P, Kothes R, Salter C J and Perillat P 2007 *Astrophys. J.* **659** 267
[6] Plaga R 1995 *Nature* **374** 430
[7] Neronov A and Semikoz D V 2007 *JETP Lett.* **85** 473
[8] Murase K, Takahashi K, Inoue S, Ichiki K and Nagataki S 2008 *Astrophys. J.* **686** L67
[9] Elyiv A, Neronov A and Semikoz D V 2009 *Phys. Rev. D* **80** 023010
[10] Dolag K, Kachelriess M, Ostapchenko S and Tomas R 2009 *Astrophys. J.* **703** 1078
[11] Dolag K, Kachelriess M, Ostapchenko S and Tomas R 2010 *Astrophys. J.* **727** L4
[12] Finke J D and Reyes L C 2015 *Astrophys. J.* **814** 20
[13] Neronov A, Taylor A M, Tchernin C and Vovk I 2013 *Astronomy and Astrophysics* **554** 5
[14] Neronov A and Semikoz D V 2009 *Phys. Rev. D* **80** 123012
[15] Abramowski A, Acero F, and Aharonian F 2012 *Astronomy and Astrophysics* **538** A103
[16] Aharonian F, Akhperjanian A G and Bazer-Bachi A R *Astronomy and Astrophysics* **470** 475
[17] Acciari V A, Aliu E and Arlen T 2009 *Astrophys. J.* **695** 2
[18] Arlen T C, Vassilev V V and Weisgarber T 2014 *ApJ* **796** 18
[19] Kachelrieß M, Ostapchenko S and Toms R 2012 *Computer Physics Communications* **183** 1036